

**Dissolution experiments of commercial PWR (52 MWd/kgU) and BWR (53 MWD/kgU)
Spent Nuclear Fuel cladded segments in bicarbonate water under oxidizing conditions.
Experimental determination of matrix and Instant Release Fraction.**

*E. González-Robles^{a**}, D. Serrano-Purroy^{b*}, R. Sureda^a, I. Casas^c, J. de Pablo^{a,c}*

^aCTM Centre Tecnològic, Plaça de la Ciència, 2, 08243 Manresa , Spain

*^bEuropean Commission, Joint Research Centre, Institute for Transuranium Elements, P.O.
Box 2340, 76125, Karlsruhe, Germany*

*^cChemical Engineering Department, Universitat Politècnica de Catalunya, Av. Diagonal 647,
08028 Barcelona, Spain*

*Corresponding author:

Daniel Serrano-Purroy

Nuclear Chemistry

European Commission, Joint Research Centre, Institute for Trans Elements

P.O. Box 2340, D-76125 Karlsruhe

Phone: +497247951417

Fax: +4972479519961

E-mail: Daniel.serrano-purroy@ec.europa.eu

**present address: Institute for Nuclear Waste Disposal (INE), Karlsruhe Institute of
Technology, P.O. Box 3640, D-76021 Karlsruhe, Germany

Abstract

The denominated instant release fraction (IRF) is considered in performance assessment (PA) exercises to govern the dose that could arise from the repository. A conservative definition of IRF comprises the total inventory of radionuclides located in the gap, fractures, and the grain boundaries and, if present, in the high burn-up structure (HBS). The values calculated from this theoretical approach correspond to an upper limit that likely does not correspond to what it will be expected to be instantaneously released in the real system. Trying to ascertain this IRF from an experimental point of view, static leaching experiments have been carried out with two commercial UO₂ spent nuclear fuels (SNF): one from a pressurized water reactor (PWR), labelled PWR, with an average burn-up (BU) of 52 MWd·kgU⁻¹ and fission gas release (FGR) of 23.1%, and one from a boiling water reactor (BWR), labelled BWR, with an average BU of and 53 MWd·kgU⁻¹ and FGR of 3.9 %.

One sample of each SNF, consisting of fuel and cladding, has been leached in bicarbonate water during one year under oxidizing conditions at room temperature (25 ± 5)°C. The behaviour of the concentration measured in solution can be divided in two according to the release rate. All radionuclides presented an initial release rate that after some days levels down to a slower second one, which remains constant until the end of the experiment. Cumulative Fraction of Inventory in Aqueous Phase (FIAP_C) values have been calculated. Results show faster release in the case of the PWR SNF. In both cases Np, Pu, Am, Cm, Y, Tc, La and Nd dissolve congruently with U, while dissolution of Zr, Ru and Rh is slower. Rb, Sr, Cs and Mo, dissolve faster than U. The IRF of Cs at 10 and 200 days has been calculated, being (3.10 ± 0.62) and (3.66 ± 0.73) for PWR fuel, and (0.35 ± 0.07) and (0.51 ± 0.10) for BWR fuel.

Keywords: spent nuclear fuel, static leaching, instant release fraction, gap contribution

PACS Codes: 89.30.Gg, 28.41.Bm, 28.41.Kw, 82.60.Hc

1. Introduction

In nuclear waste management some countries favour final geological disposal as solution for safe storage of spent nuclear fuel (SNF) [1-4]. One risk that has to be assessed is a container failure followed by groundwater ingress into the disposal vault and subsequent contact with SNF. As a consequence the SNF is leached and will release a fraction of its radionuclides inventory [2,5].

Assessing the performance of SNF in a potential future geological disposal system requires the understanding and quantification of the radionuclide release. In the past, the radionuclide release was divided into contributions from the three SNF zones: gap, grain boundary and matrix grain [1].

Radionuclides in gap and grain boundary have been considered as instant release fraction (IRF) [6,7]. This fraction includes: fission gases, volatiles (^{129}I , ^{137}Cs , ^{135}Cs , ^{36}Cl , ^{79}Se) and segregated metals (^{99}Tc , ^{107}Pd , ^{126}Sn) [8]. Recently, the tendency of increasing fuel burn-up (BU) produces ^{239}Pu by neutron capture of ^{238}U generating an external layer with a higher local BU, which presents higher porosity and fuel grain subdivision, resulting on the formation of the so-called rim zone also known as high burn-up structure (HBS) [9, 10]. This layer is observed for BU's higher than $40 \text{ MWd}\cdot\text{kgU}^{-1}$ [9-16] and is a function of BU and the irradiation temperature, being the temperature threshold 1100°C [13,15]. As a conservative approach for those SNF's, the radionuclides located in the HBS were also included in the IRF [6, 8].

The contribution of HBS to the IRF has been studied in static experiments in oxidising conditions. The first results reported by Clarens et al. [17,18] and de Pablo et al.[19] show a decreased release for the periphery of SNF pellets compared to core samples. This finding suggests some kind of stabilization against oxidative dissolution. Recent studies have observed the same effect [20-25]. Several studies have been performed to determine the

contribution of the gap and the grain boundaries contribution to IRF [26-37]. These studies were mainly focused on caesium, strontium and technetium in UOX [26-28,31,32,35-37], MOX [36] and CANDU [29-34] fuels. The gap contribution was obtained using cladded fuel segments meanwhile the grain boundary contribution was obtained by using powder samples.

In this work, the dissolution of two 10 mm rod segments (cladding + fuel) from PWR and BWR SNF's with similar BU's ($\sim 53 \text{ MWd}\cdot\text{kgU}^{-1}$) but different irradiation histories have been studied. Actinides and fission products have been determined in order to identify congruencies in release and to distinguish between gap, grain boundary and matrix contributions.

2. Experimental part

2.1 UO₂ SNF samples

Two different commercial UO₂ SNF's from a pressurized water reactor (PWR) and a boiling water reactor (BWR) were used. The relevant irradiation data are summarised in Table 1.

The cooling time period at the beginning of the experiments was 5 and 6 years, for PWR and BWR fuels, respectively.

For the present study, pieces of cladded fuel were cut from the two SNF pins, see Fig. 1. The dry cutting was performed slowly without any cooling liquid in a hot cell under nitrogen atmosphere with typical oxygen content below 1%. A cutting machine equipped with a diamond wafering blade (Buehler Isomet ® series 15HC) was used during the cutting process. Once the segments were obtained, they were characterised. The weight and the geometric parameters (length and diameter) of the samples are reported in Table 2.

2.2 Experimental set-up and procedure

The two experiments were performed in batch static conditions. The cladded SNF samples were put in a (50 ± 1) mL flask containing bicarbonate solution as a leachant, which

composition was $(1.9 \pm 0.2) \times 10^{-2}$ M NaCl and $(1.0 \pm 0.1) \times 10^{-3}$ M NaHCO₃. The solution of the experiment was equilibrated with air, leaving a head space gas of about 10 mL. In addition, to minimize the build-up of concentration gradients in the liquid phase the solution was daily shaken.

The experiments were planned to measure the initial contribution of radionuclide release. For this reason, no annealing or washing of SNF samples was carried out prior to start the experiments even if that may have as a result a high initial dissolution rate due to the possible presence of either oxidised phases or fines in the surface sample [38,39]. During the experiments the solution was fully replaced twice at 0.75 and 3.73 days to avoid possible uranium saturation and subsequently secondary phase formation. Anyhow, the solution corresponding to the both completed replenishments was analysed because provides valuable information regarding the IRF. In the following, aliquots of (3.0 ± 0.1) mL were sampled at regular time intervals (5-6 samples during the first 20 days and 4-5 more samples during the one year test). The volume was kept constant, (50 ± 1) mL, by adding fresh solution (3.0 ± 0.1) mL after each sampling.

The samples were taken without filtration. Afterwards, they were acidified and diluted with 1M HNO₃ and measured by Sector Field-ICP-MS. All samples were analysed with the addition of internal standard (Co, In, Ho and Th). A multi-element calibration was made using certified standards (Agilent Life Sciences/Chemical Analysis GmbH, Germany) at the beginning of each measurement. Calibration standards with the concentrations 0, 20, 50, 200, 600, 1000, 5000 and 20000 ppt were prepared.

The concentrations were corrected for dilution during sample preparation. Corrections for mass interferences were made taking into account also the different sensitivity factors of the interfering isotopes. Elemental concentrations were determined for each element of interest.

The detection limit for actinides was approximately $1.0 \times 10^{-12} \text{ mol} \cdot \text{L}^{-1}$ whereas the transition elements and lanthanides had a limit of detection of $1.0 \times 10^{-11} \text{ mol} \cdot \text{L}^{-1}$.

The pH, Eh and temperature were measured with an Orion 525A+ pH-meter and a gel pH Triode L/M, (9107BN, Thermo-Electron, USA) and platinum Redox electrodes, (97-78-00, Thermo-Electron, USA), respectively. The pH electrode was calibrated with commercial pH buffer solutions (METLER TOLEDO Inc., USA; pH 4.01 (Ref. 501307069), pH 7.00 (Ref. 51302047), pH 9.21 (Ref. 51302070)). Commercial pH 7.00 buffer solution was also used to calibrate the redox electrode.

The α , β and γ dose rate coming from the cladded segments of SNF to a surrounding solution was calculated in both experiment following the method described in [40]. The results in both experiments were similar obtaining a dose rate value of: 0.18 Gys^{-1} for α , 0.07 Gys^{-1} for β and $1.3 \times 10^{-3} \text{ Gys}^{-1}$ for γ .

2.3 Inventory calculation

The theoretical radionuclide inventory of the SNF's was calculated with the ORIGEN-ARP code [41] taking into account the irradiation history previously explained in section 2.1. The results are collected in Table 3, no uncertainty was given. However, in the comparison between experimental and theoretical inventories done by [42], the uncertainty of the theoretical values was estimated to be about 15%.

2.4. Solution analysis results

The concentration in solution as a function of time of 16 elements including actinides (U, Pu, Np, Am and Cm), and fission products (Rb, Sr, Y, Zr, Mo, Tc, Ru, Rh, Cs, La and Nd) was measured.

The fraction of inventory of an element i released into the aqueous phase, $FIAP_i$, was calculated according to equation 1 [43, 44]:

$$FIAP_i = \frac{m_{i, aq}}{m_{i, SNF}} = \frac{c_i V_{aq}}{m_{SNF} H_i} \quad [1]$$

where: $m_{i, aq}$ is the mass of element i in the aqueous phase and $m_{i, SNF}$ is the mass of element i in the SNF; c_i corresponds to the concentration of element i in solution ($\text{g}\cdot\text{mL}^{-1}$); V_{aq} is the volume of solution (mL), m_{SNF} is the initial mass of SNF sample (g) and H_i represents the fraction of the inventory in the SNF for the element i ($\text{g}\cdot\text{g}^{-1}$).

As explained above, two complete replenishments were done at the beginning of the experiment to avoid a likely precipitation of U. Nevertheless, these values have important information particularly about the IRF. Thereafter, the experiments were performed under pseudo-static conditions. The cumulative FIAP ($FIAP_c$) was calculated taking the two initial replenishments into account by applying equation 2:

$$FIAP_c = \frac{c_{i1^{st} rpt} V_{aq1^{st} rpt} + c_{i2^{st} rpt} V_{aq2^{st} rpt} + c_{sol(n,i)} V_{aq} \sum_{x=0}^{n-1} C_{sample(x,i)} V_{sample(x)}}{m_{SNF} H_i} \quad [2]$$

where $c_{i1^{st} rpt}$ and $c_{i2^{nd} rpt}$ correspond to the concentration in solution of element i in the 1st and 2nd replenishment, respectively; $c_{sol(n,i)}$ is the concentration in solution of element i in sample n ($\text{mol}\cdot\text{L}^{-1}$); $c_{sample(x,i)}$ is the concentration of the sample x ($\text{mol}\cdot\text{L}^{-1}$); $V_{sample(x)}$ corresponds to the volume of the aliquot x (L); and V_{aq} is the volume of solution in the static reactor (L).

The fractional release rate for an element i , FRR_i , in (d^{-1}) is given by equation 3 [24, 43]:

$$FRR_i = \frac{\Delta FIAP_i}{\Delta t} \quad [3]$$

where t is the time (d).

Finally, the fractional release normalised to uranium, FNU , is given by equation 4 [24]:

$$FNU = \frac{FIAP_i}{FIAP_U} \quad [4]$$

where $FIAP_i$ and $FIAP_U$ are the FIAP of element i and of uranium, respectively.

3. Results and discussion

3.1 Evolution of pH and Eh

The pH values showed a slight acidification from 7.6 to 7.2 ± 0.1 , whereas Eh values remained constant at values of (400 ± 50) mV (vs. NHE) in both experiments. The temperature was (25 ± 5) °C, which corresponds to normal hot cell temperature conditions.

3.2 Release of elements either congruent with or slower than matrix dissolution (U, Pu, Np, Am, Cm, Y, Zr, Ru and Rh).

The concentration in solution of these elements as function of time for PWR and BWR SNF's is plotted in Figs 2.a-3.b.

The concentration in solution of the studied elements showed a constant release rate for the first 12 days for PWR and for the first 15 days for BWR samples (see Figs 2.a-3.b). After that, a change was detected and the release rate decreased. In some cases a small drop in concentration was noticed in the solution at change of release rate time, this effect may be partially explained by an "experimental artefact". After each sampling the total volume of the solution was kept constant by adding the same amount of new solution as aliquot taken (3.0 ± 0.1 mL). If the sampling time is short and the dissolution is very slow this may result in a dilution effect (the amount taken in an aliquot could be higher than the amount released during the following sampling). Alternatively, it may be an effect related to a reduction in the total SNF surface available to be leached. The gap cracks accessible to the solution present small volume compartments with higher surface to volume ratio (S/V). In these regions, mainly in the cracks, the local concentration released into the leachate is greater than in the total bulk solution. If the concentrations exceed the solubility of a solid phase, a local precipitation process may take place blocking the gap and cracks [2,5] and reducing the concentration in solution. In addition, as a result, the total SNF surface available to be leached would be slightly smaller and a decrease in the radionuclide release would be expected.

No experimental evidence of an important secondary phase precipitation was observed.

3.2.1. Fraction of inventory in aqueous phase

The evolution of the FIAP_c follows the same trend as the measured concentrations in solution. As examples, the FIAP_c (%) of U as a function of time for PWR fuel is shown in Fig. 4.

According to these figures, it is possible to distinguish, two stages:

FIAP₁: it is an initial rapid release that comprises the initial oxidation degree of the SNF surface [30,31] as well as the possible presence of fines and/or small particles. This stage ended after 12 and 15 days in PWR and BWR SNF's, respectively. As explained in the previous section, after this stage, a decrease on FIAP_c was observed. In order to compare both SNF's a time of 10 days was chosen. The corresponding FIAP₁ (%) values at this leaching time are given in Tables 4a-4b.

Based on the data shown in Tables 4a-4b, the percentage of the U released into solution after 10 days is $(1.7 \pm 0.3) \times 10^{-2}$ and $(1.2 \pm 0.2) \times 10^{-3}$ in PWR and BWR SNF's. These values evidence a higher oxidation degree and/or presence of fines in PWR fuel than in BWR fuel.

FIAP₂: it is assumed to correspond to the matrix contribution (dissolution of grains). The value on this stage does not take FIAP₁ into account. The FIAP₂ (%) values at an arbitrary chosen time of 200 days are reported in Tables 4a-4b. After 200 days the percentage of matrix released into solution is $(3.6 \pm 0.7) \times 10^{-3}$ and $(1.3 \pm 0.3) \times 10^{-3}$ in PWR and BWR SNF's, respectively.

This difference in matrix dissolution, between both SNF's, can be explained in terms of different surface area. Although the samples used in this study have very similar physical dimensions, the PWR SNF was submitted to a higher average linear power rate in the reactor (309 W cm^{-1}) than BWR SNF (191 W cm^{-1}), this fact produces higher cracking of the fuel [50-52] and, consequently, higher surface available for corrosion. Therefore, the PWR SNF presents an "apparent" higher dissolution rate. The quantification of the matrix dissolution is

necessary in order to obtain the instant release fraction as will be explained in detail in section 3.4., although the matrix release contribution is, as expected, little significant.

In the end, the FNU was also calculated for all elements in the different stages mentioned above. Those elements which have a FNU value close to 1 indicate congruent dissolution with the UO₂ SNF matrix. That is the case, for both fuels, of the actinides and trivalent cations as Y, La and Nd. This behaviour is expected since the actinides and some fission products (Y, La and Nd) are located as solid solution within the UO₂ grains [45]. These results are in agreement with previous studies [18, 22, 24, 46-47].

On the other hand, Zr, Rh and Ru, which are found within the SNF as metallic precipitates located at the grain boundaries [45, 48] and within the matrix [49], show a FNU below 1, between 0.2 and 0.6, indicating a non-congruent, as well as slower, dissolution with SNF matrix, see Tables 4a-4b. Under these conditions the dissolution of these metallic precipitates is difficult and slower than the matrix.

3.3. Release of Rb, Sr, Mo, Tc and Cs.

The concentration in solution of these elements as function of time for PWR and BWR SNF's is plotted in Figs. 5.a-5.b.

Initially, the concentration in solution of the studied elements shows a constant release rate until 12 days for PWR and accordingly 15 days for BWR samples. Afterwards, a second slower release rate was distinguished until the end of the experiment., see Figs. 6.a-6.b. At the end of the experiments, the concentration in solution in PWR fuel were (in mol·L⁻¹): $(1.1 \pm 0.2) \times 10^{-5}$ for Rb, $(7.0 \pm 1.4) \times 10^{-6}$ for Sr, $(1.3 \pm 0.3) \times 10^{-5}$ for Mo, $(2.4 \pm 0.5) \times 10^{-6}$ for Tc and 1.1×10^{-4} for Cs. In the case of the BWR fuel the concentration in solution at the end of the experiment were (in mol·L⁻¹): $(1.0 \pm 0.2) \times 10^{-6}$ for Rb, $(1.1 \pm 0.2) \times 10^{-6}$ for Sr, $(3.4 \pm 0.7) \times 10^{-6}$ for Mo, $(1.6 \pm 0.3) \times 10^{-6}$ for Tc, $(1.2 \pm 0.2) \times 10^{-5}$ for Cs.

3.3.1. Fraction of inventory in aqueous phase

These fission products will be partly located at the gap and fractures and/or at the grain boundaries [45, 49]. A fraction of Mo and Tc will be present as ϵ -particles in the SNF [45, 48]. These fission products dissolve faster than the UO₂ SNF matrix (FNU > 1) and, therefore, comprise of the IRF. In Fig. 6 is plotted the FIAP_C (%) of Cs as a function of time in PWR and BWR SNF's.

The FIAP_C evolution of Rb, Sr, Mo, Tc and Cs as a function of time let to differentiate between 3 stages:

FIAP₁ corresponds to the intercept of the first FRR₁ at time 0. This stage represents the release mainly due to the gap and fractures, in the following called gap contribution. In addition, a certain amount of Mo and Tc, sensitive redox elements, is released as a part of the oxidised layer present on the SNF surface.

FIAP₂ corresponds to the FIAP contribution before the intersection of the two FRR regression lines subtracting the FIAP₁. At this stage, the gap contribution still dominates the dissolution behaviour. The complete gap contribution is the sum of FIAP₁ and FIAP₂. However, at the same time the grain boundaries are also dissolving and it is not possible to distinguish between both contributions. In Tables 5a-5b, the FIAP₂ values are reported at 10 days.

FIAP₃ corresponds mainly to the internal grain boundaries dissolution. The contribution was calculated at an arbitrary chosen time of 10 days. This value did not take the FIAP₁ and FIAP₂ into account, see Tables 5a-5b.

3.4 Determination of instant release fraction at time 10 and 200 days

During the dissolution process three releases occurred at the same time coming from: matrix, grain boundaries and gap and fractures dissolution [1,6,7]. The quantification of the gap and grain boundaries contribution can be determined by subtracting the matrix dissolution release.

According to the previous explanation given in section 3.3.2, the stages $FIAP_1 + FIAP_2$ will give the IRF that mainly represents the dissolution of the elements segregated to the gap between the SNF and the cladding and in the fractures of the SNF [36], and the grain boundaries more accessible to the leachate (external grain boundary). On the other hand, the $FIAP_3$ previously explained, will describe a second constant release that is slower than the first one. This second release found afterwards might be associated with internal grain boundary contribution of these elements as a consequence of the water diffusion in this internal grain boundary.

The IRF values obtained for these two regions at time 10 and 200 days are given in Table 6. The first value corresponds to the IRF due to gap + grain boundaries (external and internal) contribution, whereas values given in brackets correspond only to the internal grain boundary contribution.

As can be seen, higher gap release is obtained in the case of PWR despite both fuels have a similar BU. This effect can be associated with the difference in irradiation history. The higher the linear power rate, the higher is the fission gas release [53] and therefore the higher is the accumulation of volatiles, like Cs and Rb in the gap. It seems that the fission gas release as well as the release of volatiles radionuclides is more related to the linear power rate than to the burn-up.

Finally, after 200 days the release of the gap and the external grain boundaries is still the main release in the case of Rb and Cs. In the case of Cs the IRF after 10 and 200 days was (3.10 ± 0.62) and (3.66 ± 0.73) for PWR fuel, and (0.35 ± 0.07) and (0.51 ± 0.10) for BWR fuel. According to former data and assuming that diffusion under reactor operating conditions is a

key factor to determine the amount of Cs available for release during leaching [23], the ratio between the FGR and Cs release is 1:3 [8, 54], in the present work the ratio between the FGR and Cs release after 200 days is 1:7 for PWR fuel and 1:12 for BWR fuel, this fact suggests that other factor affect the aqueous Cs release [23]. On the other, the release due to the internal grain boundaries becomes higher as a function of time in the case of Sr, Mo and Tc. It can be conclude that these three elements are more segregated into the grain boundaries than in the gap and/or fractures.

4. Conclusions

Static leaching experiments have been carried out with two SNF's, labelled PWR and BWR, with similar BU but different irradiation history.

After an initial increase in concentration followed by all elements in both SNF's, two different concentration behaviours have been observed depending on the studied element. The first group: U, Np, Pu, Am, Cm, Zr, Y, Ru, Rh, La and Nd, showed a slight decrease of concentration in solution that could be associated to an experimental artefact or a local precipitation and finally, an increase of concentrations in solution but at lower dissolution rates than at the beginning of the experiment was observed. The second group, composed by Rb, Sr, Tc, Mo and Cs, showed an increase in concentration during all the experiment but with a decrease in dissolution rate after the first two weeks.

The FIAP and FNU values indicated matrix congruency dissolution of Np, Pu, Am, Cm, Y, La and Nd, while Zr, Ru and Rh dissolved slower than the matrix. On the other hand, Rb, Cs, Mo, Tc and Sr, presented a faster dissolution rate than the matrix. These elements constitute part of the so-called IRF.

The matrix dissolution rate was higher for PWR than BWR SNF. This might be explained by the different irradiation history. The PWR SNF was submitted to a higher average linear power rate in the reactor than BWR SNF, this fact produces higher cracking of the fuel and, consequently, higher surface available for corrosion.

The IRF at 10 and 200 days has been calculated. Higher gap release is obtained in the case of PWR than in BWR fuel, despite both fuels have a similar BU. This effect can be associated with the difference in irradiation history. The higher the linear power rate, the higher the temperature gradient during irradiation and the higher is the fission gas release and therefore the higher is the accumulation of volatiles, like Cs and Rb in the gap. It seems that the fission

gas release as well as the release of volatiles radionuclides is more related to the linear power rate than to the burn-up.

5. Acknowledgments

This work was carried out in the frame of an agreement between ITU, ENRESA, UPC and CTM. The authors acknowledge the contribution of S. Van Winckel, D.H. Wegen, D. Papaioannou as well as the technicians from the ITU Hot Cells laboratory for their technical collaboration. Aurora Martínez-Esparza is also acknowledged for her interest in this work.

6. Bibliography

- [1] L. Johnson, D.W. Shoesmith (1988) Spent Fuel in Radioactive Waste Forms for the Future. W. Lutze and R.C. Ewing, Eds. (North-Holland, Amsterdam) 635-698.
- [2] D.W. Shoesmith, Fuel corrosion process under waste disposals. *J. Nucl. Mater.*, 282 (2000), pp. 1-31.
- [3] J. Bruno, R.C. Ewing, Spent nuclear fuel. *Elements*. 2 (2006), pp. 343-349.
- [4] V. Metz, H. Geckeis*, E. González-Robles, A. Loida, C. Bube, B. Kienzler. Radionuclide behaviour in the near-field of a geological repository for spent nuclear fuel. *Radiochimica Acta*, 100 (8-9), (2012), pp.699-713.
- [5] D.W. Shoesmith, Used Fuel and Uranium dissolution studies - A review. Nuclear Waste Management Organization (NWMO), (2007), NWMO-TR-2007-03.
- [6] L. Johnson, C. Ferry, C. Poinssot, P. Lovera. Spent fuel radionuclide source-term model for assessing spent fuel performance in geological disposal. Part I: Assessment of the instant release fraction. *J. Nucl. Mater.*, 346 (2005), pp. 56-65.
- [7] C. Poinssot, C. Ferry, P. Lovera, C. Jegou, J.-M. Gras. Spent fuel radionuclide source-term model for assessing spent fuel performance in geological disposal. Part II: Matrix alteration model and global performance. *J. Nucl. Mater.*, 346 (2005), pp. 66-77.
- [8] L. Johnson, C. Ferry, C. Poinssot, P. Lovera. Estimates of the Instant Release Fraction for UO₂ and MOX fuels at t=0. Nagra, Technical Report 04-08 (2004).
- [9] H.J. Matzke, H. Blank, M. Coquerelle, K. Lassmann, I.L.F. Ray, C. Ronchi, C.T. Walker. Oxide fuel transients. *J. Nucl. Mater.*, 166 (1-2), (1989), pp. 165-178.
- [10] V.V. Rondinella, T. Wiss. The high burn-up structure in nuclear fuel. *Mater. Today*, 13 (12), (2010), pp. 24-32.

- [11] C. T. Walker, T. Kameyama, S. Kitajima, M. Kinoshita. Concerning the microstructure changes that occur at the surface of UO₂ pellets on irradiation to high burnup. *J. Nucl. Mater.*, 188 (1992), pp. 73-79.
- [12] J. Spino, K. Venix, M. Coquerelle Detailed characterisation of the rim microstructure in PWR fuels in the burn-up range 40-67 GWd/tM. *J. Nucl. Mater.*, 231 (3) (1996), pp. 179-190.
- [13] C. T. Walker. Assessment of the radial extent and completion of recrystallisation in high burn-up UO₂ nuclear fuel by EPMA. *J. Nucl. Mater.*, 275 (1) (1999), pp. 56-62.
- [14] Y.-H. Koo, B.-H. Lee, J.-S. Cheon, D.-S. Sohn. Pore pressure and swelling in the rim region of LWR high burnup UO₂ fuel. *J. Nucl. Mater.*, 295 (2-3) (2001), pp. 213-220.
- [15] T. Sonoda, M. Kinoshita, I. L. F. Ray, T. Wiss, H. Thiele, D. Pelotiero, V. V. Rondinella, H. Matzke. Transmission electron microscopy observation on irradiation-induced microstructural evolution in high burn-up UO₂ disk fuel. *Nucl. Instr. Meth. Phys. Res. B.*, 191 (1-4) (2002), pp. 622-628.
- [16] C.T. Walker, D. Staicu, M. Sheindlin, D. Papaioannou, W. Goll, F. Sontheimer. On the thermal conductivity of UO₂ nuclear fuel at a high burn-up of around 100MWd/kgHM. *J. Nucl. Mater.*, 350, (2006), pp. 19-39.
- [17] F. Clarens, D. Serrano-Purroy, A. Martínez-Esparza, D. Wegen, E. González-Robles, J. De Pablo, I. Casas, J. Giménez, B. Christiansen, J.-P. Glatz. RN fractional release of high burn-up fuels and estimation of accessible grain boundary. *Mater. Res. Soc. Symp. Proc.*, 1107 (2008), pp. 439-446.
- [18] F. Clarens, E. González-Robles, F.J. Giménez, I. Casas, J. de Pablo, D. Serrano, D. Wegen, J.P. Glatz, A. Martínez-Esparza, Effect of burn-up and high burn-up structure on spent nuclear fuel alteration, Enresa Technical Report 04/2009, Madrid, Spain, 2009.
- [19] J. de Pablo, D. Serrano-Purroy, E. González-Robles, F. Clarens A. Martínez-Esparza, D. Wegen, I. Casas, B. Christiansen, J.-P. Glatz, J. Giménez. Effect of HBS structure in Fast

Release Fraction of 48 Gwd/tU PWR fuel. Mater. Res. Soc. Symp. Proc. 1193 (2009), 613-620.

[20] C. Ferry, J.-P. Piron, A. Poulesquen, C. Poinssot. Radionuclides Release From the Spent Fuel Under Disposal Conditions: Re-evaluation of the Instant Release Fraction.. Mater. Res. Soc. Symp. Proc. 1107 (2008), 447-454.

[21] D. Roudil, C. Jegou, V. Broudic, M. Tribet, Rim instant release radionuclide inventory from French high burnup spent UOX fuel, Mat. Res. Soc. Symp. Proc., 1193 (2009), pp. 627–633.

[22] E. González-Robles. Study of Radionuclide Release in commercial UO₂ Spent Nuclear Fuels, Ph.D. Thesis. Universitat Politècnica de Catalunya, Barcelona, 2011.

[23] L. Johnson, I. Günther-Leopold, J. Kobler Waldis, H.P. Linder, J. Low, D. Cui, E. Ekeröth, K. Spahiu, L.Z. Evins Rapid aqueous release of fission products from high burn-up LWR fuel: Experimental results and correlations with fission gas release J. Nucl. Mater., 420 (2012), pp. 54–62.

[24] D. Serrano-Purroy, I. Casas, E. González-Robles, J.P. Glatz, D.H. Wegen, F. Clarens, J. Giménez, J. de Pablo, A. Martínez-Esparza. Dynamic leaching studies of 48MWd/kgU UO₂ commercial spent nuclear fuel under oxic conditions J. Nucl. Mater., 434 (2013), 451-460.

[25] T. Fanghänel, V. V. Rondinella, J.-P. Glatz, T. Wiss, D. H. Wegen, T. Gouder, P. Carbol, D. Serrano-Purroy, D. Papaioannou. Reducing Uncertainties Affecting the Assessment of the Long-Term Corrosion Behavior of Spent Nuclear Fuel. Inorganic chemistry. *Inorg. Chem.*, 2013, 52 (7), pp 3491–3509.

[26] V. M. Oversby, H. F. Shaw, Spent fuel performance data: An analysis of data relevant to the NNWSI project. Livermore, California, USA: Lawrence Livermore National Laboratory, Technical Report ACID-20926, 1987, pp. 56.

- [27] C. N. Wilson,. Results from NNWSI Series 2 bare fuel dissolution tests. Richland, Washington, USA: Pacific Northwest Laboratory Report, PNL-7169, 1990.
- [28] R.S. Forsyth, L.O. Werme. Spent fuel corrosion and dissolution. *J. Nucl. Mater.* 190 (1992), pp. 3-19.
- [29] S. Stroes-Gascoyne, J.C. Tait, R.J. Porth, J.L. McConnell, T.R. Barnsdale, S. Watson. Measurements of grain-boundary inventories of ^{137}Cs , ^{90}Sr and ^{99}Tc in used CANDU fuel. *Mat. Res. Soc. Symp. Proc.*, 294 (1993), pp. 41-53.
- [30] S.Stroes-Gascoyne, J.C. Tait, R.J. Porth, J.L. McConnell, W.J Lincoln. Release of ^{14}C from the gap and grain-boundary regions of used candu fuels to aqueous solutions. *Waste Management* , 14 (5), (1994), pp. 385-392.
- [31] R. S. Forsyth, U-B. Eklund, L.O. Werme. A study of fission product migration and selective leaching by means of a power-bumo test. *Mat. Res. Soc. Symp. Proc.*, 333 (1994), pp. 385-390.
- [32] W. J. Gray, C.N. Wilson. Spent fuel dissolution studies FY 1991 to 1994. Pacific Northwest National Laboratory. Technical Report, PNL -10540 (1995).
- [33] S. Stroes-Gascoyne, D. L. Moir, M. Kolar, R. J. Porth, J. L. McConnell and A. H. Kerr.Measurement of gap and grain-boundary inventories of ^{129}I in used CANDU fuels. *Mat. Res. Soc. Symp. Proc.*, 353 (1), (1995), pp. 625-631.
- [34] S. Stroes-Gascoyne Measurements of instant-release source terms for ^{137}Cs , ^{90}Sr , ^{99}Tc , ^{129}I and ^{14}C in used CANDU fuels. *J. Nucl. Mater.*, 238 (1996), pp. 264-277.
- [35] W.J. Gray, Inventories of I-129 and Cs-137 in the gaps and grain boundaries of LWR spent fuels, *Mat. Res. Soc. Symp. Proc.*, 556 (1999), pp. 478-494.
- [36] D. Roudil, C. Jegou, V. Broudic, B. Muzeau, S. Peugeot, X. Deschanel. Gap and grain boundaries inventories from pressurized water reactor spent fuels. *J. Nucl. Mater.*, 362 (2007), pp. 411–415.

- [37] Kim, S. S., Kang, K. C., Choi, J. W., Seo, H. S., Kwon S. H., Cho. W. J. Measurement of the gap and grain boundary inventories of Cs, Sr and I in domestic used PWR Fuels. J. Kor. Radioac. Waste Soc., 5(1) (2007), pp. 79-84.
- [38] J.A. Serrano , J.P. Glatz, E.H. Toscano, D. Papaioannou, J. Barrero, M. Coquerelle. Influence of low temperature air oxidation on the dissolution behaviour of UO₂ and MOX spent fuel. J. Nucl. Mater., 271-273 (1998), pp. 573-576.
- [39] J.A. Serrano , J.P. Glatz, E.H. Toscano, D. Papaioannou, J. Barrero, M. Coquerelle. Influence of low temperature air oxidation on the dissolution behaviour of LWR spent fuel. J. Nucl. Mater., 294 (2001), pp. 339-343.
- [40] F. Nielsen, M. Jonsson, Geometrical α - and β -dose distributions and production rates of radiolysis products in water in contact with spent nuclear fuel. J. Nucl. Mater., 359 (2006), pp 1-7.
- [41] Bowman, S.W., Leal, L.C. ORIGEN-ARP Automatic Rapid Process For Spent Fuel depletion, Decay, And Source Term Analysis, "NUREG/CR-0200 Revision 6. Volume1, Section D1, ORNL/NUREG/CSD-2/V1/R6, Oak Ridge, Tennessee (USA) (2000).
- [42] Y. Cao, Y. Gohar, C. H. M. Broeders. MCNPX Monte Carlo burnup simulations of the isotope correlation experiments in the NPP Obrigheim. Ann. Nucl. Energy, 2010, vol. 37, pp. 1321-1328.
- [43] R.S. Forsyth, L.O. Werme, J. Bruno. The corrosion of spent UO₂ fuel in synthetic groundwater. J. of Nucl. Mater., 138 (1986) pp. 1-15.
- [44] B. Hanson, R.B. Stout. Re-examining the dissolution of Spent Fuel: a comparison of different Methods for calculating Rates. Mater. Res. Soc. Symp. Proc. 824 (2004) 89-94.
- [45] H. Kleykamp. The chemical state of the fission products in oxide fuels. J. Nucl. Mater., 131 (1986), pp. 221-246.

- [46] R. Forsyth, An Evaluation of Results from the Experimental Programme Performed in the Studsvik Hot Cell Laboratory, in, Svensk Kärnbränslehantering AB, Stockholm, Sweden, 1997, pp. 81
- [47] D. Serrano-Purroy, I. Casas, E. González-Robles, J.P. Glatz, D.H. Wegen, F. Clarens, J. Giménez, J. de Pablo, A. Martínez-Esparza. Dynamic leaching studies of 48 MWd/kgU UO₂ commercial spent nuclear fuel under oxidic conditions J. Nucl. Mater., 434 (1-3), (2013), pp. 451-460.
- [48] J.I. Bramman, R.M. Sharpe, D. Thom, G. Yates. Metallic Fission-product inclusions in irradiated oxide fuels. J. Nucl. Mater., 25 (1968), pp. 201-215.
- [49] D. Cui, J. Low, C.J. Sjöstedt, K. Spahiu. On Mo-Ru-Tc-Pd-Rh-Te alloy particles extracted from spent fuel and their leaching behaviour under Ar and H₂ atmospheres. Radiochimica Acta, 92 (2004) 551-555.
- [50] J.C. Wood, B.A. Surette, I. Aitchison. Pellet cladding interaction - Evaluation of lubrication by graphite. J. Nucl. Mater., 88 (1)(1980), pp. 81-94.
- [51] M. Oguma . Cracking and relocation behaviour of nuclear fuel pellets during rise to power. Nucl. Eng. Des., 76 (1983), pp. 35-45.
- [52] Y.-H. Koo, B.-H. Lee, D.-S. Sohn. Analysis of fission gas release and gaseous swelling in UO₂ fuel under the effect of external restraint. J. Nucl. Mater., 280 (1) (2000), pp. 86-98.
- [53] K. Kamimura, FP gas release behavior of high burnup MOX fuels for thermal reactors, in: Proc. of Technical Committee Meeting on Fission Gas Release and Fuel Rod Chemistry Related to Extended Burnup, Pembroke, Ontario, Canada, 28 April-1 May 1992, IAEA-TECDOC-697, 1992, pp. 82 – 87.
- [54] K.A. Lassman, A. Schubert, J. van der Laar, C.T. Walker, On the diffusion coefficient of cesium in UO₂ fuel, fission gas behavior of water reactor fuels, in: Seminar Proc. 26-29 September 2000, NEA, 2002, pp. 321-334.

Table 1. Fuel irradiation history of PWR and BWR spent nuclear fuels.

SNF	Average BU (MWd/kgU)	Irradiation time (days)	Number of cycles	Average linear power (W cm⁻¹)	FGR (%)
PWR	52	975	3	309	23.1
BWR	53	1368	5	191	3.9

Table 2. Summary of physical characterisation of cladded segment samples (PWR and BWR).

SNF	PWR	BWR
Weight (g)	8.4296 ± 0.0001	7.5911 ± 0.0001
Length (mm)	10.4 ± 0.1	10.2 ± 0.1
Diameter (mm)	10.0 ± 0.1	10.0 ± 0.1

Table 3. Calculated inventory in ($\mu\text{g g}^{-1} \text{g}_{\text{SNF}}^{-1}$), using ORIGEN-ARP code, for PWR and BWR SNF's,

Element	PWR ($\mu\text{g}_{\text{element}} \cdot \text{g}_{\text{SNF}}^{-1}$)	BWR ($\mu\text{g}_{\text{element}} \cdot \text{g}_{\text{SNF}}^{-1}$)
Rb	500	510
Sr	1190	1170
Y	660	660
Zr	5100	5200
Mo	4700	4800
Tc	1100	1100
Ru	2900	2900
Rh	600	580
Cs	3500	3530
La	1700	1700
Nd	5500	5600
U	823000	824000
Np	700	600
Pu	9700	8600
Am	400	500
Cm	60	70

Table 4a Elemental FIAP (%) and FNU for transuranium elements in PWR SNF. FIAP_{at time 0}, FIAP₁ and FNU₁ at 10 days; FIAP₂ and FNU₂ at 200 days.

Element	FIAP _{at time 0}	FIAP ₁ (%)	FIAP ₂ (%)	FNU ₁	FNU ₂
Y	$(1.2 \pm 0.2) \times 10^{-2}$	$(1.8 \pm 0.4) \times 10^{-2}$	$(4.9 \pm 1.0) \times 10^{-3}$	1.0 ± 0.4	1.4 ± 0.6
Zr	$(6.2 \pm 1.2) \times 10^{-3}$	$(9.7 \pm 1.9) \times 10^{-3}$	$(5.8 \pm 1.2) \times 10^{-4}$	0.6 ± 0.2	0.2 ± 0.1
Ru	$(2.1 \pm 0.4) \times 10^{-3}$	$(2.5 \pm 0.5) \times 10^{-3}$	$(7.6 \pm 1.5) \times 10^{-4}$	0.1 ± 0.06	0.2 ± 0.1
Rh	$(3.0 \pm 0.6) \times 10^{-3}$	$(3.9 \pm 0.8) \times 10^{-3}$	$(7.3 \pm 1.5) \times 10^{-4}$	0.2 ± 0.1	0.2 ± 0.1
La	$(1.2 \pm 0.2) \times 10^{-2}$	$(1.9 \pm 0.4) \times 10^{-2}$	$(3.5 \pm 0.7) \times 10^{-3}$	1.1 ± 0.4	1.0 ± 0.4
Nd	$(1.4 \pm 0.3) \times 10^{-2}$	$(2.0 \pm 0.4) \times 10^{-2}$	$(5.1 \pm 1.0) \times 10^{-3}$	1.2 ± 0.5	1.4 ± 0.6
U	$(1.3 \pm 0.3) \times 10^{-2}$	$(1.7 \pm 0.3) \times 10^{-2}$	$(3.6 \pm 0.7) \times 10^{-3}$	1.0 ± 0.4	1.0 ± 0.4
Np	$(1.3 \pm 0.3) \times 10^{-2}$	$(1.9 \pm 0.4) \times 10^{-2}$	$(2.4 \pm 0.5) \times 10^{-3}$	1.1 ± 0.5	0.7 ± 0.3
Pu	$(1.4 \pm 0.3) \times 10^{-2}$	$(2.0 \pm 0.4) \times 10^{-2}$	$(2.3 \pm 0.5) \times 10^{-3}$	1.2 ± 0.5	0.6 ± 0.3
Am	$(2.0 \pm 0.4) \times 10^{-2}$	$(2.8 \pm 0.6) \times 10^{-2}$	$(3.5 \pm 0.7) \times 10^{-3}$	1.6 ± 0.6	1.0 ± 0.4
Cm	$(2.9 \pm 0.6) \times 10^{-2}$	$(3.8 \pm 0.8) \times 10^{-2}$	$(4.5 \pm 0.9) \times 10^{-3}$	2.2 ± 0.9	1.3 ± 0.5

Table 4b Elemental FIAP (%) and FNU for transuranium elements in BWR SNF. FIAP_{at time 0}, FIAP₁ and FNU₁ at 10 days; FIAP₂ and FNU₂ at 200 days.

Element	FIAP _{at time 0}	FIAP ₁ (%)	FIAP ₂ (%)	FNU ₁	FNU ₂
Y	$(1.9 \pm 0.4) \times 10^{-4}$	$(4.7 \pm 0.9) \times 10^{-3}$	$(2.9 \pm 0.3) \times 10^{-3}$	3.9 ± 1.5	2.2 ± 0.9
Zr	$(4.2 \pm 0.9) \times 10^{-4}$	$(1.2 \pm 1.2) \times 10^{-3}$	$(7.9 \pm 0.8) \times 10^{-4}$	1.0 ± 0.4	0.6 ± 0.2
Ru	$(3.0 \pm 0.6) \times 10^{-5}$	$(2.2 \pm 0.4) \times 10^{-4}$	$(2.0 \pm 0.3) \times 10^{-4}$	0.2 ± 0.1	0.2 ± 0.1
Rh	$(6.2 \pm 1.2) \times 10^{-5}$	$(4.8 \pm 0.9) \times 10^{-4}$	$(2.1 \pm 0.2) \times 10^{-4}$	0.4 ± 0.2	0.2 ± 0.1
La	$(2.8 \pm 0.6) \times 10^{-4}$	$(3.5 \pm 0.7) \times 10^{-3}$	$(2.6 \pm 0.3) \times 10^{-3}$	2.8 ± 1.1	1.9 ± 0.8
Nd	$(2.3 \pm 0.5) \times 10^{-4}$	$(2.4 \pm 0.5) \times 10^{-3}$	$(2.6 \pm 0.3) \times 10^{-3}$	1.9 ± 0.8	1.9 ± 0.8
U	$(3.2 \pm 0.6) \times 10^{-4}$	$(1.2 \pm 0.2) \times 10^{-3}$	$(1.3 \pm 1.3) \times 10^{-3}$	1.0 ± 0.4	1.0 ± 0.4
Np	$(4.0 \pm 0.8) \times 10^{-4}$	$(1.9 \pm 0.4) \times 10^{-3}$	$(1.3 \pm 1.3) \times 10^{-3}$	1.6 ± 0.6	1.0 ± 0.4
Pu	$(4.1 \pm 0.8) \times 10^{-4}$	$(1.8 \pm 0.4) \times 10^{-3}$	$(6.0 \pm 0.9) \times 10^{-4}$	1.4 ± 0.6	0.7 ± 0.3
Am	$(5.9 \pm 1.2) \times 10^{-4}$	$(2.5 \pm 0.5) \times 10^{-3}$	$(2.0 \pm 2.0) \times 10^{-3}$	2.0 ± 0.8	1.5 ± 0.6
Cm	$(5.9 \pm 1.2) \times 10^{-4}$	$(3.2 \pm 0.6) \times 10^{-3}$	$(2.3 \pm 0.2) \times 10^{-3}$	2.6 ± 1.1	1.7 ± 0.7

Table 5a. Elemental FIAP (%) and FNU for Rb, Sr, Mo, Tc and Cs in PWR SNF.

Element	FIAP ₁ (%)	FIAP ₂ (%)	FIAP ₃ (%)	FNU ₁	FNU ₂	FNU ₃
Rb	$(7 \pm 1) \times 10^{-1}$	$(2.1 \pm 0.4) \times 10^{-1}$	$(1.2 \pm 0.2) \times 10^{-2}$	52 ± 21	48 ± 19	64 ± 26
Sr	$(7 \pm 1) \times 10^{-1}$	$(9 \pm 2) \times 10^{-2}$	$(5 \pm 1) \times 10^{-3}$	0.6 ± 0.2	21 ± 8	28 ± 11
Mo	$(3.3 \pm 0.7) \times 10^{-2}$	$(1.3 \pm 0.3) \times 10^{-2}$	$(1.9 \pm 0.4) \times 10^{-3}$	3 ± 1	3 ± 1	11 ± 4
Tc	$(2.2 \pm 0.4) \times 10^{-2}$	$(5 \pm 1) \times 10^{-3}$	$(1.3 \pm 0.3) \times 10^{-3}$	1.7 ± 0.7	1.2 ± 0.5	7 ± 3
Cs	2.6 ± 0.5	0.6 ± 0.1	$(2.3 \pm 0.5) \times 10^{-2}$	203 ± 81	148 ± 59	129 ± 52

Table 5b. Elemental FIAP (%) and FNU for Rb, Sr, Mo, Tc and Cs in BWR SNF.

Element	FIAP ₁ (%)	FIAP ₂ (%)	FIAP ₃ (%)	FNU ₁	FNU ₂	FNU ₃
Rb	$(1.5 \pm 0.3) \times 10^{-3}$	$(6 \pm 1) \times 10^{-2}$	$(2.3 \pm 0.5) \times 10^{-3}$	46 ± 18	37 ± 15	35 ± 14
Sr	$(1.7 \pm 0.3) \times 10^{-4}$	$(2.4 \pm 0.5) \times 10^{-3}$	$(1.7 \pm 0.3) \times 10^{-3}$	5 ± 2	15 ± 6	26 ± 10
Mo	$(3.2 \pm 0.6) \times 10^{-3}$	$(2.5 \pm 0.5) \times 10^{-4}$	$(1.6 \pm 0.3) \times 10^{-3}$	10 ± 4	2 ± 1	23 ± 9
Tc	$(1.2 \pm 0.2) \times 10^{-4}$	$(2.0 \pm 0.4) \times 10^{-4}$	$(3.0 \pm 0.6) \times 10^{-3}$	4 ± 2	1.2 ± 0.5	45 ± 18
Cs	$(2.4 \pm 0.5) \times 10^{-2}$	$(1.7 \pm 0.3) \times 10^{-1}$	$(7 \pm 1) \times 10^{-3}$	741 ± 296	106 ± 42	105 ± 42

Table 6. IRF at 10 and 200 days of Rb, Sr, Mo, Tc and Cs, for PWR and BWR SNF's. The first value represents the total IRF that includes gap + grain boundaries (external and internal) contribution at 10 and 200 days. Values in brackets correspond only to the internal grain boundary contribution.

SNF	PWR		BWR	
BU	52		53	
Element	IRF (%) at 10 days	IRF (%) at 200days	IRF (%) at 10 days	IRF (%) at 200days
Rb	0.82 ± 0.17 (1.1 ± 0.2)x10 ⁻³	1.08 ± 0.22 (2.3 ± 0.5)x10 ⁻¹	0.05 ± 0.01 (2.3 ± 0.5)x10 ⁻³	0.12 ± 0.02 (4.6 ± 0.9)x10 ⁻²
Sr	0.07 ± 0.01 (4.8 ± 0.9)x10 ⁻³	0.18 ± 0.04 (9.9 ± 2.0)x10 ⁻²	0.017 ± 0.003 (1.7 ± 0.3)x10 ⁻³	0.06 ± 0.01 (3.5 ± 0.7)x10 ⁻²
Mo	0.03 ± 0.01 (1.8 ± 0.4)x10 ⁻³	0.07 ± 0.01 (3.9 ± 0.8)x10 ⁻²	0.004 ± 0.001 (1.5 ± 0.3)x10 ⁻³	0.033 ± 0.007 (3.1 ± 0.6)x10 ⁻²
Tc	0.010 ± 0.002 (1.1 ± 0.2)x10 ⁻³	0.03 ± 0.001 (2.5 ± 0.5)x10 ⁻²	0.0012 ± 0.0002 (3.0 ± 0.6)x10 ⁻³	0.06 ± 0.01 (6.1 ± 1.2)x10 ⁻²
Cs	3.10 ± 0.62 (2.3 ± 0.5)x 10 ⁻²	3.66 ± 0.73 (4.6 ± 0.9)x 10 ⁻¹	0.35 ± 0.07 (7.0 ± 1.4)x 10 ⁻³	0.51 ± 0.10 (1.4 ± 0.3)x10 ⁻¹

Figure Captions

Figure 1. Cross section of the PWR (right) and BWR (left) clad segments.

Figure 2a. Concentration in solution of actinides as a function of time for PWR fuel. The vertical lines at 0.75 and 3.73 days correspond to the 1st and 2nd replenishment. The error bars for some elements are smaller than the symbols: the uncertainty in all cases is 20 %

Figure 2b. Concentration in solution of actinides as a function of time for BWR fuel. The vertical lines at 0.75 and 3.73 days correspond to the 1st and 2nd replenishment. The error bars for some elements are smaller than the symbols: the uncertainty in all cases is 20 %.

Figure 3a. Concentration in solution of: Y, Zr, Ru, Rh, La and Nd as a function of time for PWR fuel. The vertical lines at 0.75 and 3.73 days correspond to the 1st and 2nd replenishment. The error bars for some elements are smaller than the symbols: the uncertainty in all cases is 20 %.

Figure 3b. Concentration of: Y, Zr, Ru, Rh, La and Nd as a function of time for BWR fuel. The vertical lines at 0.75 and 3.73 days correspond to the 1st and 2nd replenishment. The error bars for some elements are smaller than the symbols: the uncertainty in all cases is 20 %.

Figure 4. Evolution of FIAP_c (%) for U as a function of time in for PWR fuel

Figure 5a. Concentration in solution of: Rb, Sr, Mo, Tc and Cs as a function of time for PWR fuel. The vertical lines at 0.75 and 3.73 days correspond to the 1st and 2nd replenishment. The error bars for some elements are smaller than the symbols: the uncertainty in all cases is 20 %.

Figure 5b. Concentration in solution of: Rb, Sr, Mo, Tc and Cs as a function of time for PWR fuel. The vertical lines at 0.75 and 3.73 days correspond to the 1st and 2nd replenishment. The error bars for some elements are smaller than the symbols: the uncertainty in all cases is 20 %.

Figure 6. Evolution of FIAP_c (%) for Cs as a function of time in for PWR fuel

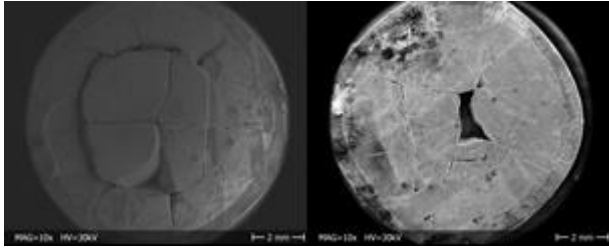


Figure 1. Cross section of the PWR (right) and BWR (left) cladded segments.

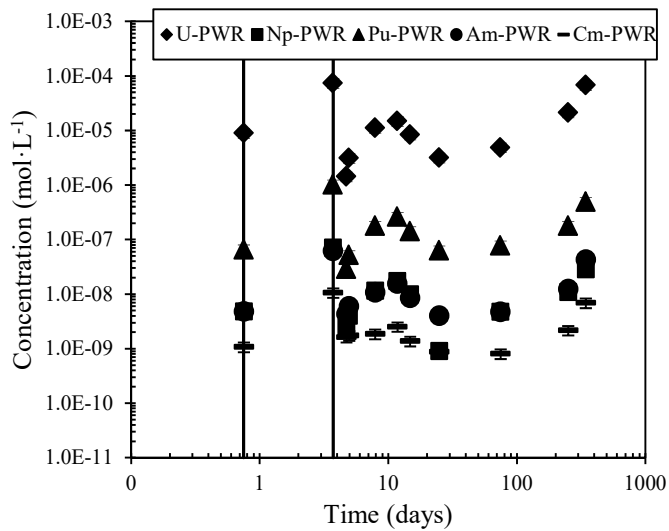


Figure 2a. Concentration in solution of actinides as a function of time for PWR fuel. The vertical lines at 0.75 and 3.73 days correspond to the 1st and 2nd replenishment. The error bars for some elements are smaller than the symbols: the uncertainty in all cases is 20 %

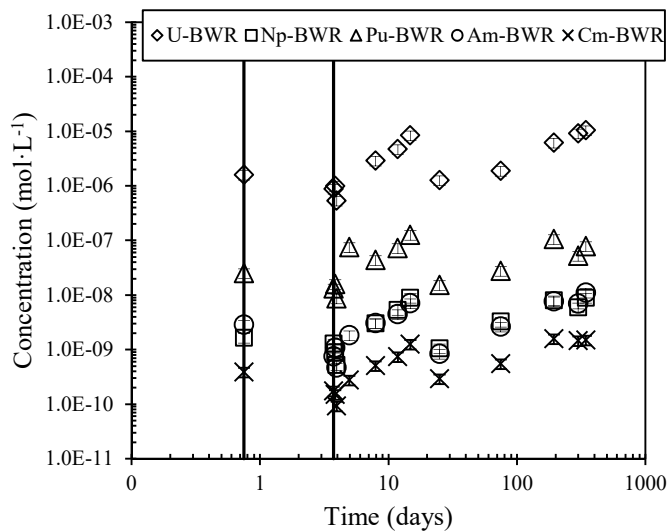


Figure 2b. Concentration in solution of actinides as a function of time for BWR fuel. The vertical lines at 0.75 and 3.73 days correspond to the 1st and 2nd replenishment. The error bars for some elements are smaller than the symbols: the uncertainty in all cases is 20 %.

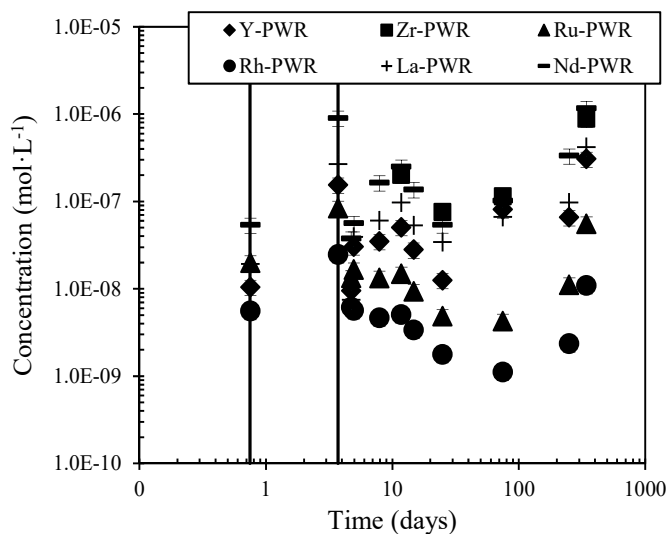


Figure 3a. Concentration in solution of: Y, Zr, Ru, Rh, La and Nd as a function of time for PWR fuel. The vertical lines at 0.75 and 3.73 days correspond to the 1st and 2nd replenishment. The error bars for some elements are smaller than the symbols: the uncertainty in all cases is 20 %.

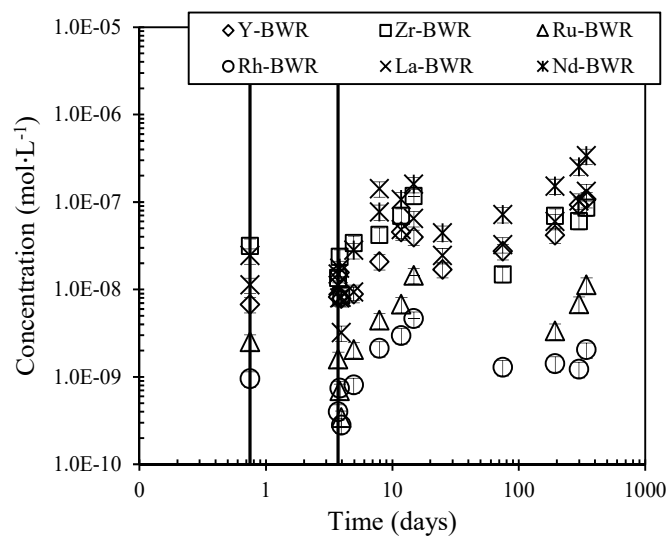


Figure 3b. Concentration of: Y, Zr, Ru, Rh, La and Nd as a function of time for BWR fuel. The vertical lines at 0.75 and 3.73 days correspond to the 1st and 2nd replenishment. The error bars for some elements are smaller than the symbols: the uncertainty in all cases is 20 %.

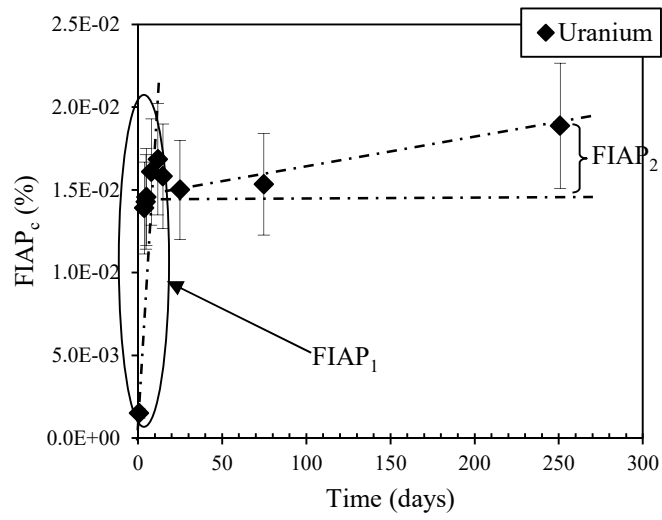


Figure 4. Evolution of FIAP_c (%) for U as a function of time in for PWR fuel.

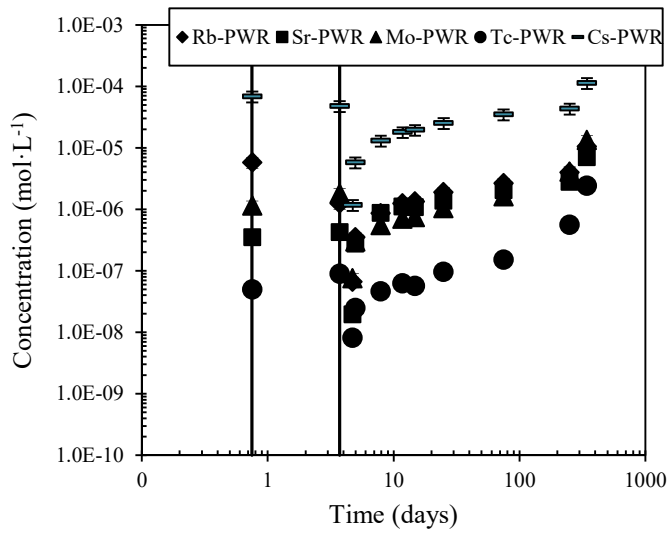


Figure 5a. Concentration in solution of: Rb, Sr, Mo, Tc and Cs as a function of time for PWR fuel. The vertical lines at 0.75 and 3.73 days correspond to the 1st and 2nd replenishment. The error bars for some elements are smaller than the symbols: the uncertainty in all cases is 20 %.

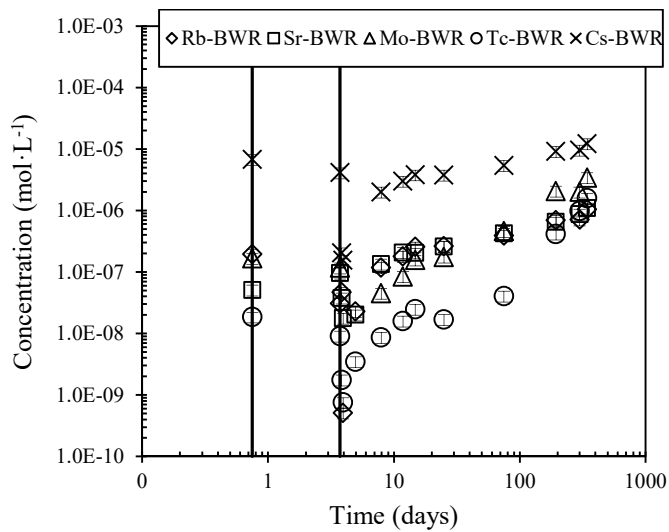


Figure 5b. Concentration in solution of: Rb, Sr, Mo, Tc and Cs as a function of time for PWR fuel. The vertical lines at 0.75 and 3.73 days correspond to the 1st and 2nd replenishment. The error bars for some elements are smaller than the symbols: the uncertainty in all cases is 20 %.

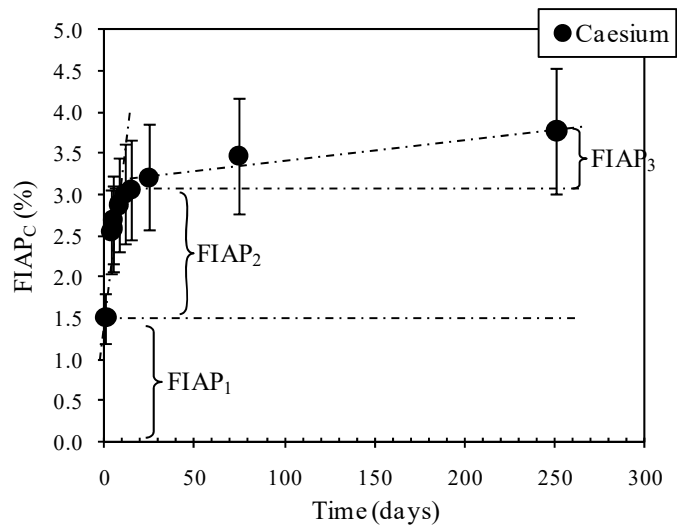


Figure 6. Evolution of FIAP_c (%) for Cs as a function of time in for PWR fuel